WILEY | Hindawi

*Research Article*

# Available Transfer Capability Assessment of Multiarea Power Systems with Conditional Generative Adversarial Network

**Xiangfei Meng** [iD],[1] **Lina Zhang,**[1] **Xin Tian** [iD],[1] **Hongqing Chu,**[1] **Yao Wang,**[1] **and Qingxin Shi** [iD][2]

[1]*Economic & Technology Research Institute of State Grid Shandong Electric Power Company, Jinan, Shandong 250021, China*
[2]*School of Electrical & Electronics Engineering, North China Electric Power University, Beijing 102206, China*

Correspondence should be addressed to Xin Tian; aatianxin@163.com

Available transfer capability (ATC) is an important measurement index to evaluate the security margin of interconnected power grids and serve as a reference for the transmission right transaction. In modern power systems, ATC is affected by the transmission network topology, renewable power output uncertainty, and load demand uncertainty. Traditional works usually model the power source-load uncertainty by using robust optimization, interval optimization, or chance-constraint optimization, which cannot fully reflect the probabilistic distribution of the daily source-load uncertainty. This paper proposes an ATC assessment methodology based on the typical stochastic scenarios of renewable output and load demand of multiarea power systems. Furthermore, the conditional generative adversarial network (CGAN) algorithm is adopted to generate and select representative scenario sets based on historical raw data, which can fully reflect the usual operating condition of a system with high renewable energy penetration. The scenario set that is fed into the ATC assessment model can fully characterize the impact of source-load uncertainty on daily ATC. Finally, the proposed method is verified by a modified three-area IEEE 9-bus system and a real-world provincial power system.

## 1. Introduction

In the electricity market, ensuring economic operation under power system security constraints has become an urgent problem for operators and participants. Available transfer capability (ATC) represents the remaining power transfer capacity on condition that the secure and stable operation of the power system is guaranteed. In other words, ATC approximately evaluates the safety and stability margin of the current operating point. Therefore, ATC is not only an important basis for electricity market participants to carry out transmission right transactions [1–3] but also a boundary condition for the power system expansion planning [4]. In modern power systems with high penetration of renewable energy and multiple types of loads, it is of great significance to propose an ATC evaluation method to satisfy electricity market operation.

Traditionally, researchers proposed multiple calculation methods of ATC under deterministic source and load parameters, including the linear distribution factor method, continuous power flow method, and optimal power flow (OPF) method [5–7]. The OPF method aims to maximize the power flow of interarea tie lines with the constraints of power flow balance, security, and stability criteria. Thus, the power system ATC in a deterministic operating state can be directly obtained by solving the OPF problem.

The modern power system with high renewable energy penetration is characterized by uncertain renewable power output, long-distance power transmission, and complex load composition. Therefore, the uncertainty of wind/photovoltaic power generation and the uncertainty of the load lead to the fluctuation of power transfer between different areas [8, 9]. As a result, the ATC of interareas tie lines can be uncertain and difficult to obtain. Regarding the uncertainty of renewable power generation and load demand, researchers have proposed methods based on robust optimization [10], interval optimization [11], and optimization including chance constraints [12]. Considering the uncertainty of wind farm output

and load demand, a robust ATC evaluation model was proposed, which included a master problem of determining total transfer capability and two subproblems of solving capacity benefit margin (CBM) and transmission reliability margin (TRM). In comparison, the authors of [10] propose a robust ATC evaluation model considering reliability marginal terms with a focus on the impact of dynamic line rating (DLR) instruments on ATC. An interval optimization-based model was proposed for ATC evaluation, which considers the range of uncertain variables [11]. In this model, the maximum of the ATC lower bound and the minimum of the upper bound were presented by a lower boundary (optimistic) model and an upper boundary (pessimistic) model, respectively. Then, the feasible region of ATC was obtained by simplifying the solution with the strong duality theory. The study in [12] established the joint probability distribution function of multiple wind farms' power output and incorporated the uncertainty with chance constraints. Then, the chance-constrained programming problem was converted into an equivalent linear programming one. In the studies of [13, 14], a prediction error probability model of wind power output was developed and a bilevel optimization model considering regional wind power output correlation was proposed, where the upper layer maximizes inter-regional ATC and the lower layer minimizes generation cost and risk cost. In [15], an ATC evaluation framework of an intraday market was developed based on the existing Var sources. In [16], the ATC evaluation was modelled as a nonlinear OPF problem, which adopts an iterative decomposition-coordination approach based on the constrained augmented Lagrangian method. In addition to static security constraints, the small-signal stability constraint is considered in the ATC evaluation [17]. Considering the rigorously small-signal stability model is complex, this study proposed a sequential quadratic programming method combined with gradient sampling (GS). The study in [18] proposed an online ATC evaluation method considering the uncertainty of renewable energy output. The method maximizes the difference between the benefits and risks of the power increase. Moreover, ATC is an important basis for transmission system expansion planning and renewable power plant planning [4]. Therefore, electric power utility companies need to assess the ATC based on the power grid topology and power source-load distribution. The study in [19] presented a methodology for reinforcing an existing transmission network, considering wind power investment to enhance ATC, and proposes a bilevel structure where the upper level is the joint transmission expansion planning (TEP) and wind power investment, while the lower level calculates the ATC.

To summarize, the ATC of modern power systems is not only determined by a set of security constraints but also characterized by the spatial-temporal probability distribution of renewable power output and load demand. Therefore, the key problems of ATC evaluation are the generation of source-load random scenarios. Traditional methods based on robust optimization or interval optimization are relatively easy to solve. However, they only provide the distribution range of the ATC and can neither provide its probability distribution nor average value. Therefore, the transaction right trading in the electricity market lacks an accurate boundary. Although the traditional Monte Carlo simulation method can generate many stochastic scenarios of renewable energy and load, the computation workload is high and it cannot effectively classify and screen the scenarios [20]. Consequently, it is difficult to obtain the probability distribution of the ATC of multiarea power systems.

Based on this motivation, this paper proposes a multi-time-step ATC evaluation method based on typical scenario sets of renewable power output and load demand. First, the calculation method of the maximal transfer case considering the security index of multiregional power system operation is proposed, and the ATC evaluation model is developed. Second, according to the multidimensional uncertainty of renewable energy and load, the conditional generative adversarial network (CGAN) method is adopted to generate and screen the typical daily scenario sets. Hence, the sets' system baseline operating points are obtained for ATC evaluation. Finally, the probability distribution of ATC is calculated by the optimal dispatch model based on the stochastic scenario sets, which serves as an important basis for power system expansion planning and developing trading mechanisms of the electricity market.

The remaining parts of this paper are organized as follows. Section 2 proposes the ATC calculation model based on the stochastic baseline case. Section 3 introduces the CGAN-based method to generate and screen the stochastic scenarios of renewable energy and load. The verification study based on a three-area IEEE system and a real-word system is presented in Section 4, considering the stochastic scenario set. Section 5 concludes the whole paper and introduces future research directions.

## 2. ATC Assessment Model

Given the network topology, nodal load, power growth mode, and other operation parameters, the power system ATC indicates determining the maximum additional power that can be transmitted based on the existing transmission power of the key lines of the power system.

*2.1. ATC Evaluation Framework.* ATC is the difference between total transfer capacity (TTC) and existing transfer commitments (ETC), capacity benefit margin (CBM), and transmission reliability margin (TRM) [12]. TTC is the maximum transferred power between areas of the system under various safety constraints such as bus voltage and line capacity [20]. ETC is the transfer of power between areas of the system under the baseline case. Generally, CBM and TRM are constants determined by the area dispatch and control centre [21]. Therefore, CBM and TRM are ignored in this paper for simplification. In a given renewable energy-load scenario, the objective function under the maximum transfer case is established as follows [9]:

$$\min . \sum_{t \in T} \left[ \alpha c_i P_{i,t}^G - \beta \sum_{i \in G} \left( P_{i,t}^{Gm} - P_{i,t}^G \right) \right]. \tag{1}$$

In this study, the increased power is only provided by the source area. The first term of the objective function is the day-ahead economic dispatching cost of the generators in the case of known new energy output and load demand, and the second term is the sum of the generators' output margin. The maximum transfer case of the power system indicates the operating state where the thermal generators reach their maximum power output (not necessarily the generators' upper limit) under the system security operating constraints. The constraint conditions include line power flow constraints, nodal voltage constraints, frequency security constraints, and transient stability constraints. It is noted that since the objective function and constraints are determined by stochastic scenarios, the subscript $s$ used to describe scenarios in power and voltage variables is omitted.

According to the random scenario set, the ATC of the system in the time slot $t$ has a probability distribution, and its mean value is calculated by the following equation:

$$\text{ATC}_s = \frac{1}{T} \sum_{t=1}^{T} \text{ATC}_{t,s}. \tag{2}$$

When the random source-load scenario sets are sufficient, their probability distribution can represent the distance from the baseline case to the maximum transfer case under stochastic scenarios.

### 2.2. Operation Constraints of Power System.
In the power system, starting from the typical baseline case, the exchanged power between different areas is continuously increased by adjusting the generator output and nodal load until the safety constraints reach the limit, and the maximum transfer case of the system is obtained. ATC is the difference of the exchanged power in areas between the baseline case and the maximum transfer case. The operation constraints of the system are summarized as follows.

### 2.2.1. Baseline Case.
Considering the power flow constraints and static security constraints, the operating constraints of the baseline case are given by the following equations:

$$\begin{cases} P_{i,t} = P_{i,t}^G + P_{i,t}^W - P_{i,t}^D, \\ \\ Q_{i,t} = Q_{i,t}^G + 0 - Q_{i,t}^D, \end{cases} \tag{3}$$

$$Q_{i,t}^D = \lambda_i P_{i,t}^D, \tag{4}$$

$$\begin{cases} P_{i,t} = \sum_{\substack{j=1 \\ j \neq i}}^{\text{NB}} \left[ B_{ij}^2 \left( \delta_{i,t} - \delta_{j,t} \right) + B_{ij}^1 \left( V_{i,t} - V_{j,t} \right) \right], \\ \\ Q_{i,t} = \sum_{\substack{j=1 \\ j \neq i}}^{\text{NB}} \left[ -B_{ij}^1 \left( \delta_{i,t} - \delta_{j,t} \right) + B_{ij}^2 \left( V_{i,t} - V_{j,t} \right) \right], \end{cases} \tag{5}$$

$$B_{ij}^1 = \frac{r_{ij}}{r_{ij}^2 + x_{ij}^2} B_{ij}^2 = \frac{x_{ij}}{r_{ij}^2 + x_{ij}^2}, \tag{6}$$

$$\begin{cases} -S_{ij}^{\max} \leq B_{ij}^2 \left( \delta_{i,t} - \delta_{j,t} \right) + B_{ij}^1 \left( V_{i,t} - V_{j,t} \right) \leq S_{ij}^{\max}, \\ -0.5 S_{ij}^{\max} \leq -B_{ij}^1 \left( \delta_{i,t} - \delta_{j,t} \right) + B_{ij}^2 \left( V_{i,t} - V_{j,t} \right) \leq 0.5 S_{ij}^{\max}, \end{cases} \tag{7}$$

$$V^{\min} \leq V_{i,t} \leq V^{\max}, \tag{8}$$

$$\begin{cases} P_i^{\text{Gmin}} \leq P_{i,t}^G \leq P_i^{\text{Gmax}}, \\ Q_i^{\text{Gmin}} \leq Q_{i,t}^G \leq Q_i^{\text{Gmax}}, \end{cases} \tag{9}$$

$$\begin{cases} P_{i,t,s}^G - P_{i,t+1}^G \leq r P_i^{\text{Gmax}}, \\ -r P_i^{\text{Gmax}} \leq P_{i,t}^G - P_{i,t+1}^G. \end{cases} \tag{10}$$

Constraint (3) is the active and reactive power balance constraint of nodes. It is assumed that the wind farm only generates active power. The power factor is assumed to be constant, and the reactive power variable is replaced by the real power, as given by (4). Constraint (5) is the linearized power flow equation, in which the amplitude and phase angle of the nodal voltage can be solved simultaneously. The equivalent admittance $B_{ij}^1$, $B_{ij}^2$ of the power flow equation is calculated by the resistance and inductance of the line, as given by equation (6) [22]. The capacity constraint of the line is nonlinear. However, considering that the active nodal load and the active power transmitted by lines are generally greater than the reactive nodal load and the reactive power through lines, the capacity constraint of the line $(i, j)$ is approximately represented by equation (7) [23]. Constraint (8) enforces the voltage limit of each node. Constraint (9) represents the output limit of the generator $i$ at time $t$, indicating that the active output of the generator $i$ at time $t$ should be between its upper and lower limits. Constraint (10) represents the ramping down and ramping up constraints per unit time of the generator $i$, respectively.

*2.2.2. Maximum Transfer Case.* Similar to the baseline case, the power system still satisfies the nodal power balance constraint, power flow constraint, nodal voltage constraint, and thermal power plant constraint. Therefore, the constraints (3), (5), (7)–(10) are rewritten as follows:

$$\begin{cases} P_{i,t} = P_{i,t}^{Gm} + P_{i,t}^W - P_{i,t}^{Dm}, \\ Q_{i,t} = Q_{i,t}^{Gm} + 0 - Q_{i,t}^{Dm}, \end{cases} \tag{11}$$

$$\begin{cases} P_{i,t}^m = \sum_{j=1,j\neq i}^{NB} \left[ B_{ij}^2 \left( \delta_{i,t}^m - \delta_{j,t}^m \right) + B_{ij}^1 \left( V_{i,t}^m - V_{j,t}^m \right) \right], \\ Q_{i,t}^m = \sum_{j=1,j\neq i}^{NB} \left[ -B_{ij}^1 \left( \delta_{i,t}^m - \delta_{j,t}^m \right) + B_{ij}^2 \left( V_{i,t}^m - V_{j,t}^m \right) \right], \end{cases} \tag{12}$$

$$\begin{cases} -S_{ij}^{max} \leq B_{ij}^2 \left( \delta_{i,t}^m - \delta_{j,t}^m \right) + B_{ij}^1 \left( V_{i,t}^m - V_{j,t}^m \right) \leq S_{ij}^{max}, \\ -0.5S_{ij}^{max} \leq -B_{ij}^1 \left( \delta_{i,t}^m - \delta_{j,t}^m \right) + B_{ij}^2 \left( V_{i,t}^m - V_{j,t}^m \right) \leq 0.5S_{ij}^{max}, \end{cases} \tag{13}$$

$$V^{min} \leq V_{i,t}^m \leq V^{max}, \tag{14}$$

$$\begin{cases} P_i^{Gmin} \leq P_{i,t}^{Gm} \leq P_i^{Gmax}, \\ Q_i^{Gmin} \leq Q_{i,t}^{Gm} \leq Q_i^{Gmax}, \end{cases} \tag{15}$$

$$\begin{cases} P_{i,t,s}^{Gm} - P_{i,t+1}^{Gm} \leq rP_i^{Gmax}, \\ -rP_i^{Gmax} \leq P_{i,t}^{Gm} - P_{i,t+1}^{Gm}, \end{cases} \tag{16}$$

$$\begin{cases} P_{i,t}^G \leq P_{i,t}^{Gm}, & i \in SR, \\ P_{i,t}^G = P_{i,t}^{Gm}, & i \in SK, \end{cases} \tag{17}$$

$$\begin{cases} P_{i,t}^D = P_{i,t}^{Dm}, & i \in SR, \\ P_{i,t}^D \leq P_{i,t}^{Dm}, & i \in SK, \end{cases} \tag{18}$$

where variables $P_{i,t}^m$, $Q_{i,t}^m$, $P_{i,t}^{Gm}$, $Q_{i,t}^{Gm}$, $P_{i,t}^{Dm}$, $Q_{i,t}^{Dm}$, $\delta_{i,t}^m$, and $V_{i,t}^m$ in the maximum transfer case correspond to $P_{i,t}$, $Q_{i,t}$, $P_{i,t}^G$, $Q_{i,t}^G$, $P_{i,t}^D$, $Q_{i,t}^D$, $\delta_{i,t}$, and $V_{i,t}$ in the baseline case, respectively. Since ATC measures the incremental potential of interarea power transfer, this paper makes two assumptions regarding the maximum transfer case: (1) the power output increment from the baseline case to the maximum transfer case is totally caused by thermal power plants in the source area and (2) the load increment from baseline operating point to extreme operating point is totally caused by the load in the sink area. This assumption is widely adopted in many early literature [8, 11]. Based on the assumption, the variation relation between baseline case and maximum transfer case is given by constraints (17)-(18).

*2.3. Stochastic Scenario Set.* The baseline operating point is a set of operating parameters, including the power plant output, load demand, and line switching state. In the provincial-level

power system, the baseline case is affected by the distribution of power flow, which is naturally determined by time-varying renewable power plant output and load demand. Therefore, for the purpose of comprehensive ATC assessment, it is necessary to establish the typical scenario set of supply-demand based on the historical raw data.

$$\mathbf{S}^0 = \left\{ \mathbf{S}^W, \mathbf{S}^D \right\},$$
$$\mathbf{S}^W = \left\{ P_1^W, P_2^W, \cdots, P_i^W \right\}, i \in W, \qquad (19)$$
$$\mathbf{S}^D = \left\{ P_1^D, P_2^D, \cdots, P_i^D \right\}, i \in D,$$

where $P_i^W = [P_{i,1}^W, P_{i,2}^W, \cdots, P_{i,24}^W]^T$ and $P_i^D = [P_{i,1}^D, P_{i,2}^D, \cdots, P_{i,24}^D]^T$. The detailed stochastic supply-demand scenario generation will be discussed in Section 3.

## 3. CGAN-Based Scenario Generation

A set of representative scenarios of renewable power and load is generated based on extracting the features of the historical raw data. Generative adversarial networks (GANs) leverage deep neural networks (DNNs) to express complex nonlinear relationships (the generator) and to classify complex signals (the discriminator). The key insight of GANs is to set up a mini-max two-player game between the generator DNN and the discriminator DNN. Therefore, GAN is an effective approach to ATC assessment.

During each training epoch, the generator updates its weights to generate "fake" samples trying to "fool" the discriminator network, while the discriminator tries to tell the difference between true historical samples and generated samples. This training will continue until the discriminator is unable to tell the difference. Based on GAN, CGAN transmits additional condition information to the discrimination model and generation model as part of the input layer. Figure 1 shows the general architecture of CGAN's training procedure under our specific setting [24].

### 3.1. Problem Formulation.
In a large system, multiple renewable resources need to be considered at the same time. It is essential to simultaneously generate multiple scenarios for a given group of geographical-close sites. The generated scenarios should capture both the temporal and spatial correlations between the resources, as well as the marginal distribution of each individual resource.

In order to generate scenarios with distinct properties, the given properties are incorporated into the training process by labelling each training sample with an assigned label that represents the event. Specifically, this work uses a label vector **y** to classify and record certain properties in an observation $x_j$. This method is proposed to generate scenarios conditioned on the label $y$, where samples with the same label are expected to exhibit similar properties. The objective is to train a generative model based on CGAN using historical conditional power generation data $\{x_j | y_j\}$, $j = 1, 2, \ldots, N$ as a training set.

### 3.2. Conditional Generative Adversarial Networks.
The architecture of the CGAN is depicted in Figure 1. Assume observations $x_j^t$ for times $t \in T$ of renewable power are available for each power plant $j = 1, 2, \ldots, N$. Let $\mathbb{P}_X$ denote the true distribution, which is unknown and hard to model. Suppose there is an access to a group of noise vector input $z$ under a known distribution $Z \sim \mathbb{P}_Z$ that is easily sampled from (e.g., jointly Gaussian). The goal is to transform a sample $z$ drawn from $\mathbb{P}_Z$ such that it follows $\mathbb{P}_X$. This is accomplished by simultaneously training two deep neural networks: the generator network and the discriminator network. Let $G(\cdot; \theta^{(G)})$ and $D(\cdot; \theta^{(D)})$ denote the generator and discriminator function parametrized by $\theta^{(G)}$ and $\theta^{(D)}$, the weights of two neutral networks, respectively. The generator and discriminator are defined as follows [24].

### 3.2.1. Generator.
The generator is trained to take a batch of inputs and to output realistic scenarios with a series of up-sampling operations. Suppose that $Z$ is a random variable with a distribution $\mathbb{P}_Z$. Then, $G(Z; \theta^{(G)})$ is a new random variable, whose distribution is denoted as $\mathbb{P}_G$.

### 3.2.2. Discriminator.
The discriminator is trained simultaneously with the generator. The discriminator takes input samples from real historical data or generator, and by taking a series of operations of downsampling using another deep neural network, the discriminator outputs a continuous value $P_{\text{real}}$ that measures to what extent the input samples belong to $\mathbb{P}_X$. The discriminator can be expressed as follows:

$$p_{\text{real}} = D\left( x; \theta^{(D)} \right). \qquad (20)$$

The discriminator is trained to distinguish between $\mathbb{P}_X$ from $\mathbb{P}_G$ and to maximize the difference between $E[D(X)]$ (real data) and $E[D(G(Z))]$ (generated data).

With the objectives for the discriminator and generator, the next step is to formulate the loss function $L_G$ for the generator and $L_D$ for the discriminator to train them, and a small $L_G$ reflects the generated samples as realistically as possible from the discriminator's perspective. Similarly, a small $L_D$ indicates a discriminator that is good at telling the difference between generated scenarios and historical scenarios. Thus, $L_D$ and $L_G$ can be written as follows:

$$L_G = -\mathbb{E}_Z [D(G(Z))], \qquad (21)$$

$$L_D = -\mathbb{E}_X [D(X)] + \mathbb{E}_Z [D(G(Z))]. \qquad (22)$$

The combination of (21) and (22) forms a two-player mini-max value function and establishes a game between the generator and discriminator so that they can be trained simultaneously. The mini-max objective of the game can be interpreted as the dual of the so-called Wasserstein distance. The purpose of CGAN is to obtain two random variables $\mathbb{P}_X (D(X))$ and $\mathbb{P}_Z (D(G(Z)))$ close to each other. It is given by the following equation:
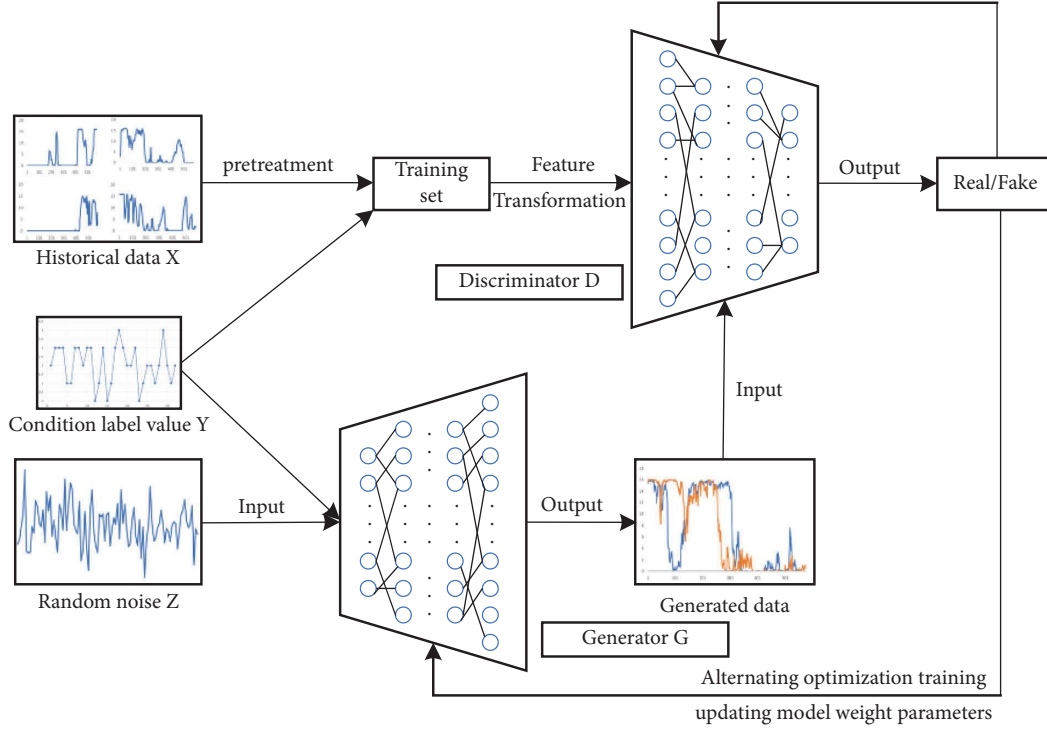
FIGURE 1: The architecture for CGANs used for wind scenario generation.

$$W(D(X), D(G(Z))) = \sup_{\theta^{(D)}} \{\mathbb{E}_X[D(X)] - \mathbb{E}_Z[D(G(Z))]\}. \tag{23}$$

Wasserstein distance directly calculates the distance between two distributions $\mathbb{P}_G$ and $\mathbb{P}_X$. Since the purpose is to generate scenarios that reflect the variability of renewables generation and load demand, the training based on Wasserstein distance leads to capture all the modes in training samples.

Furthermore, it is necessary to obtain scenarios "conditioned on" certain classes of events. Conditional generation is carried out by incorporating more information into the training procedure of GANs, such that the generated samples conforming to the same properties as certain class of training samples. Hence, the event labels are combined with training samples, and the objective for $G$ is to generate samples under a given class. Thus, the problem can be written as follows [25]:

$$\min_{\theta^{(G)}} \max_{\theta^{(D)}} W(D(X), D(G(Z))) = \mathbb{E}_X[D(X|y)] - \mathbb{E}_Z[D(G(Z|y))]. \tag{24}$$

Class labels are assigned based on user-defined classification metrics. There are three types of conditional values set in this study:

(1) Historical meteorological data with time attribute

(2) Spatial characteristics such as station location, topography, and landform

(3) Output characteristics of power plants

As shown in Figure 2, the generator is trained to generate the required typical scenarios. Both $D(x; \theta^{(D)})$ and $G(z; \theta^{(G)})$ consist of differentiable functions with distinct neural layers.

The gradient descent training method is employed to optimize the performance of these two networks. A batch update training method was used, the RMSProp algorithm was applied as a gradient descent optimizer to adaptively adjust the learning rate, and this algorithm was used for weight updating of the discriminator and generator neural networks [26]. Clipping is also applied to constrain $D(x; \theta^{(D)})$ and to prevent gradients explosion [27].

Furthermore, the generator accepts random noise and conditional values as inputs, while the discriminator accepts wind power output curve or load curve and conditional values as inputs. The wind power output data or load data of
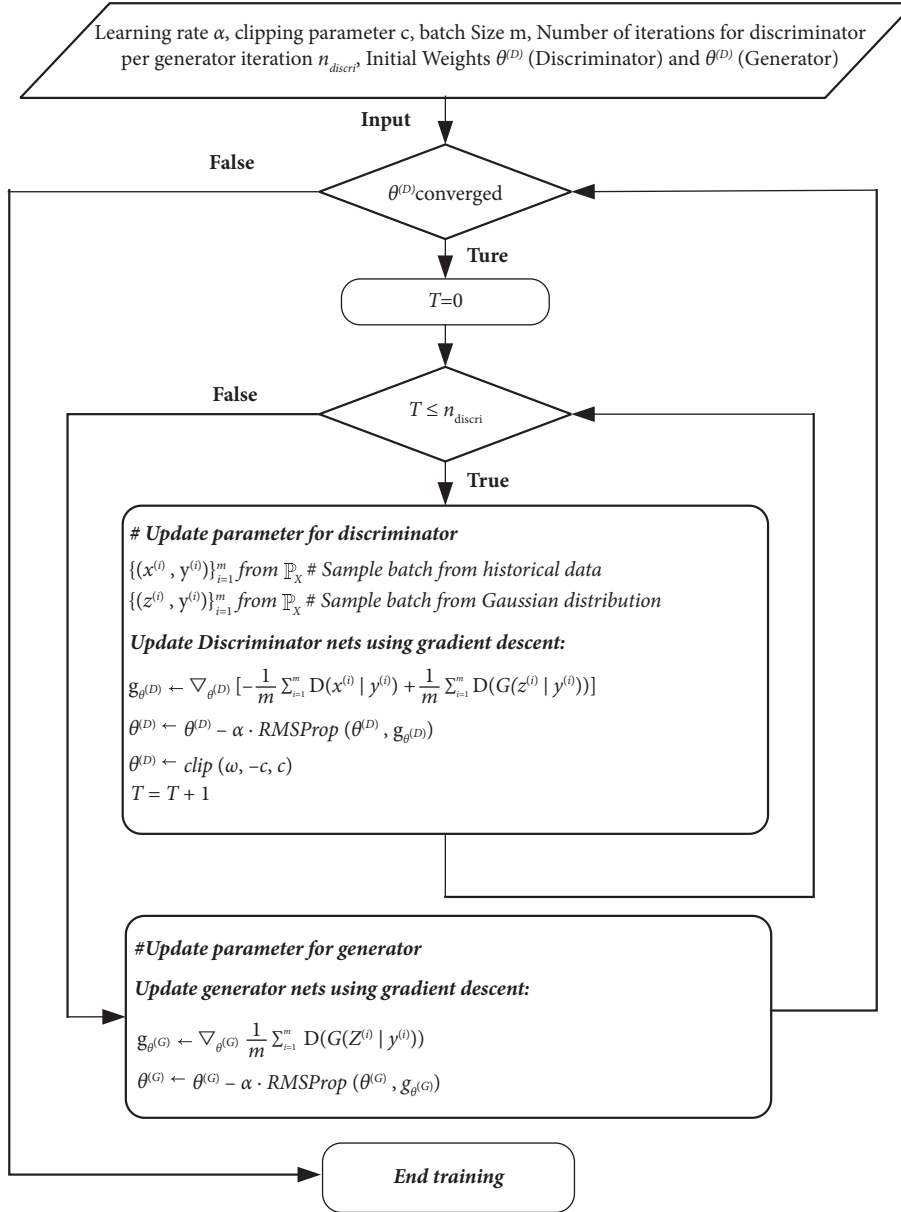
FIGURE 2: The flowchart of scenario generation based on CGAN.

each substation are decomposed into a matrix of $N \times T$, where $N$ and $T$ represent the number of scenario curves and the number of daily curve sample points, respectively. Five and three are selected as classification labels for wind power and load, respectively. Then, one-hot coding is utilized to convert these discrete classification labels into binary vectors. This method can effectively introduce the condition information into the training process of the generator and discriminator. As a result, both the generator and discriminator can obtain the condition information during training to better generate and discriminate sample data.

These label values are horizontally spliced into the historical data matrix to input the real data and condition values as training sets into the discriminator for training. Similarly, it is assumed that the Gaussian noise, being sampled randomly from the normal distribution, has the same dimension $N \times T$. The next step is to concatenate the Gaussian noise horizontally with the label value after one-hot coding and send the Gaussian noise as input to the generator for training. In each training, we select appropriate batches of noise and real data, and we input them together with condition label values into the generator and discriminator, respectively. The "fake" data generated by the generator will be further input into the discriminator for discrimination, and the discriminator will output the value of Wasserstein distance as its discrimination result. To improve the accuracy of the discriminator network and to make the training process more stable, the generator is trained every four times after training the discriminator. This alternative updating method can balance the training of

the generator and discriminator and ensure their mutual influence to achieve a better training effect. Through continuous iterative training, the Wasserstein distance will gradually approach 0. Meanwhile, the generator can accurately generate wind power output or load scenarios under different conditions.

## 4. Case Study

This section validates the proposed ATC assessment method by using two multiarea power systems, including a modified IEEE 9-bus system and a real-world provincial system. The stochastic source-load scenario set is discussed in 4.1 and applicable to two test cases. Then, the simulation results are presented and analyzed in 4.2. The computational tasks are performed on a personal computer with an Intel Core i7 processor (2.60 GHz) and 8 GB RAM, and the code is implemented via MATLAB-based IBM ILOG CPLEX Optimization Studio V12.10.0.

*4.1. Stochastic Scenario Generation.* This subsection presents the historical raw data of wind power plant and substation-level load in a coastal area in China. The representative scenario set of daily wind power and load demand is generated using the CGAN introduced in Section 3. First, eight representative daily scenarios (named as W1~W8) of wind power are generated based on 365 days of historical data, as shown in Figure 3(a), in which the vertical axis represents the p.u. power output regarding the installed capacity of a wind power plant. Second, eight representative scenarios of load demand (named as L1~L8) are generated based on 365 days of historical data, as shown in Figure 3(b), in which the vertical axis represents the p.u. power output regarding the yearly peak load of this substation. Figure 4 indicates that after a certain number of iterations, the empirical Wasserstein distance between the distribution of the real sample and the generated samples gradually converges to zero. Therefore, the CGAN-based scenario generation method can achieve high convergence accuracy and extract the best representative daily source-load scenario from massive historical data.

Generally, it is essential to evaluate the ATC based on the representative baseline cases of high thermal power plant output and low thermal power plant output. Therefore, the set of representative scenarios is generated and classified into four types, as summarized in Table 1. Different scenarios indicate different baseline operating states. For example, in Type 1, the output of most thermal power plants is relatively high, and it can be inferred that the margin of thermal power increase is low.

*4.2. ATC Assessment Result*

*4.2.1. IEEE 9-Bus System.* The test system is shown in Figure 5, which consists of two 9-bus systems. The source area and sink area share a similar structure with attached loads and generators. Both the source area and sink area contain thermal power plants and wind power plants. Detailed parameters of thermal power plants are listed in Table 2 [28]. The installed capacity of three wind power plants that are integrated into bus 4, 13, and 19 is 300, 500, and 600 MVA, respectively. In the source area, the total rated power of thermal power plants is larger than its peak load while, in the sink area, the total rated power of thermal power plants is smaller than its peak load. Besides, the wind power penetration of both areas is 28.40%. Therefore, the power is transferred from the source area to the sink area no matter how the wind power fluctuates. The daily profiles of wind power output and load demand are generated by the CGAN algorithm.

The ATC assessment is conducted based on four types of representative wind-load scenarios. In the multiobjective optimization model, the weighted factor $\alpha$ and $\beta$ are set to be 0.2 and 0.8, respectively. For each of these four types of typical scenarios, a typical day is selected, and the time-varying ATC assessment results are displayed in Figure 6. The maximum average ATC value is 1195.510 MW, which occurs in the scenario of type 4 (i.e., large wind power generation-low load). Under the low load condition, the transmission network has more ATC to meet the power supply-demand due to a large number of wind power generations. The minimum average value of ATC is 517.600 MW and appears in type 1 (i.e., small wind power generation-high load scenario). The reason is that in the case of high load and low wind power output, the ATC of the transmission network is bounded, and there may be a risk of power supply shortage. Therefore, the uncertainties of load and wind power output are the key factors affecting ATC.

Among each type of scenario, the daily average standard deviation of ATC can be obtained, as shown in Table 3. The probability distribution of ATC suggests the margin for increasing the thermal generator output under the uncertain wind power and load demand of a regional power system. The result provides the power market participants with the potential capacity of tie lines.

The thermal generator outputs under four types of scenarios are shown in Figure 7. It can be observed that generators in area 2 under the four types of scenarios are close to full capacity. Here, type 1-$G_3$ reaches the maximum output from 7 a.m. to 9 p.m., type 2-$G_4$ reaches the maximum output from 8 a.m. to 10 p.m., type 3-$G_4$ reaches the maximum output from 5 p.m. to 11 p.m., and type 4-$G_6$ reaches the maximum output during the typical day.

The proposed ATC evaluation method is compared with the interval optimization method which consists of optimistic and pessimistic models [11] by using the same test system (in Figure 5). The result is shown in Figure 8. It can be observed that in terms of calculation accuracy, the results obtained by the proposed method always fall within the range of the interval optimization method. Compared with providing only a possible range for ATC, the proposed method provides higher calculation accuracy. Therefore, the proposed method is more practical in power system operation and planning.

*4.2.2. A Read-World Power System.* The ATC assessment method is implemented on the 44-node read-world power system for further verification, as depicted in Figure 9.
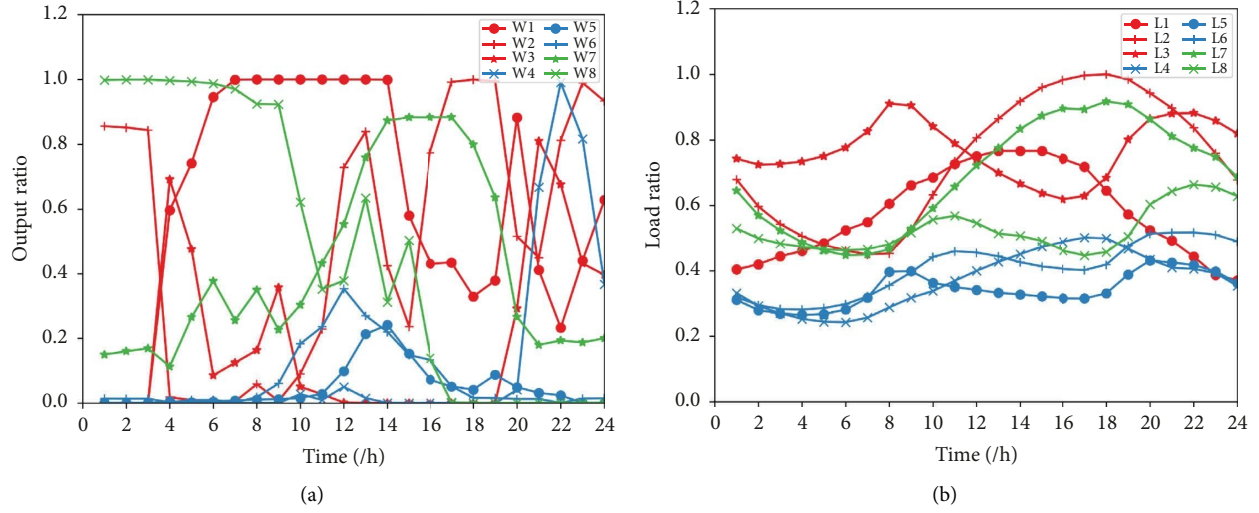
(a)



(b)

FIGURE 3: Stochastic scenarios of source and load. (a) Wind power output stochastic scenarios sets. (b) Load stochastic scenarios sets.
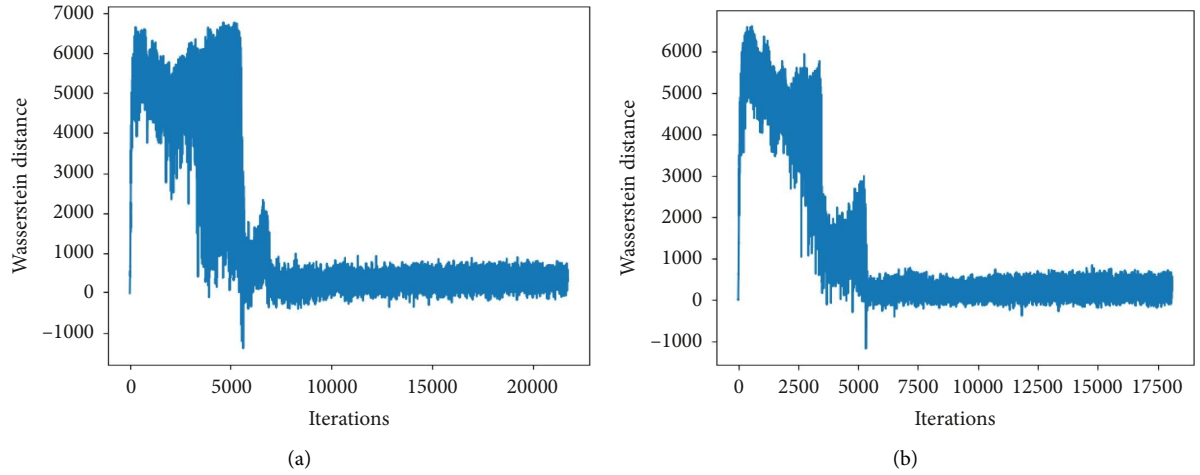


(a)



(b)

FIGURE 4: Error of forecast. (a) Wind power output. (b) Load.

TABLE 1: Summary of 4 types of scenarios.

| Type | Wind power output | Load demand | Thermal power output in the baseline case |
|---|---|---|---|
| 1 | Low | High | High |
| 2 | High | High | Medium |
| 3 | Low | Low | Medium |
| 4 | High | Low | Low |

This system consists of interconnected source areas, sink areas, and a wind power area, with four tie lines facilitating the interconnection. In this system, there are 15 thermal power plants with their parameters detailed in Table 4 and six wind turbine units located at bus 3, bus 12, bus 26, bus 42, bus 43, and bus 44, respectively, and the installed capacity of wind power accounts for 28.694% of the maximum power supply load.

The weighting coefficients $\beta$ and $\alpha$ are maintained at a ratio of 4, as per the previous case. For the four typical scenarios, ATC was evaluated sequentially, and the results obtained are shown in Figure 10. For large systems, under low loads, the value of available transmission capacity changes less and is more stable. The highest available transfer capability scenario remains type 4, and the smallest scenario remains type 1.
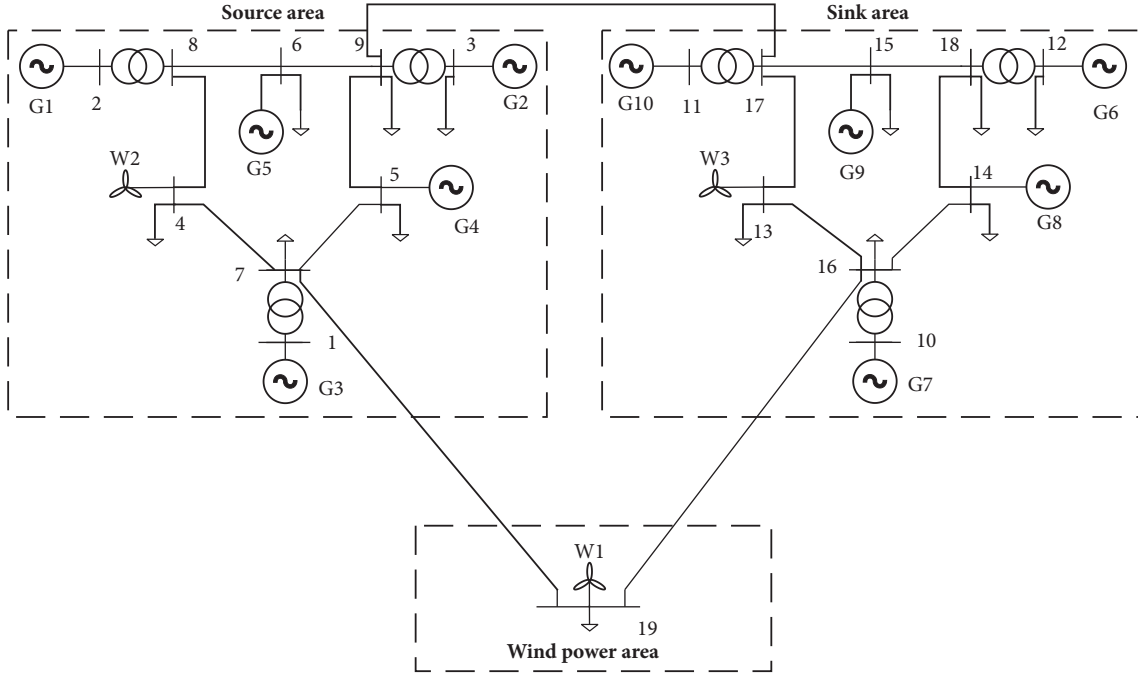
FIGURE 5: Multiarea 9-node system diagram.

TABLE 2: Parameters of thermal power plants for 9-node system.

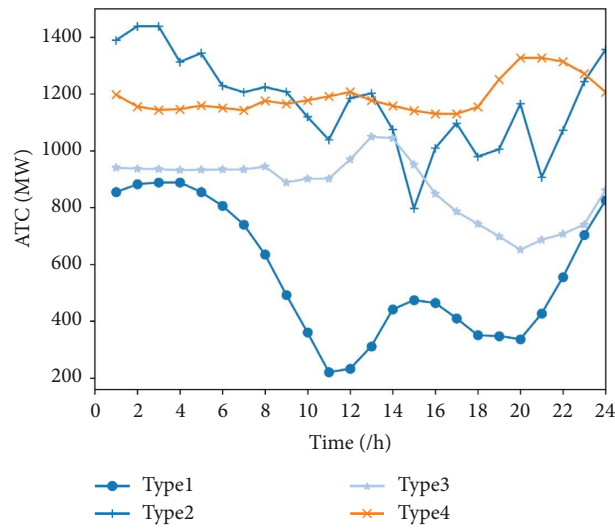| Bus no. | $c$ | $P_{\max}$ (MVA) | $P_{\min}$ (MVA) |
|---------|-----|------------------|------------------|
| $G_1$ | 2 | 700 | 240 |
| $G_2$ | 1 | 550 | 200 |
| $G_3$ | 1.2 | 600 | 180 |
| $G_4$ | 1 | 530 | 150 |
| $G_5$ | 2 | 500 | 150 |
| $G_6$ | 1 | 250 | 100 |
| $G_7$ | 1.2 | 300 | 150 |
| $G_8$ | 1.2 | 350 | 180 |
| $G_9$ | 1.5 | 250 | 100 |
| $G_{10}$ | 1.2 | 370 | 150 |



FIGURE 6: Day-ahead ATC evaluation result for 9-node system.

TABLE 3: Probabilistic distribution of ATC.

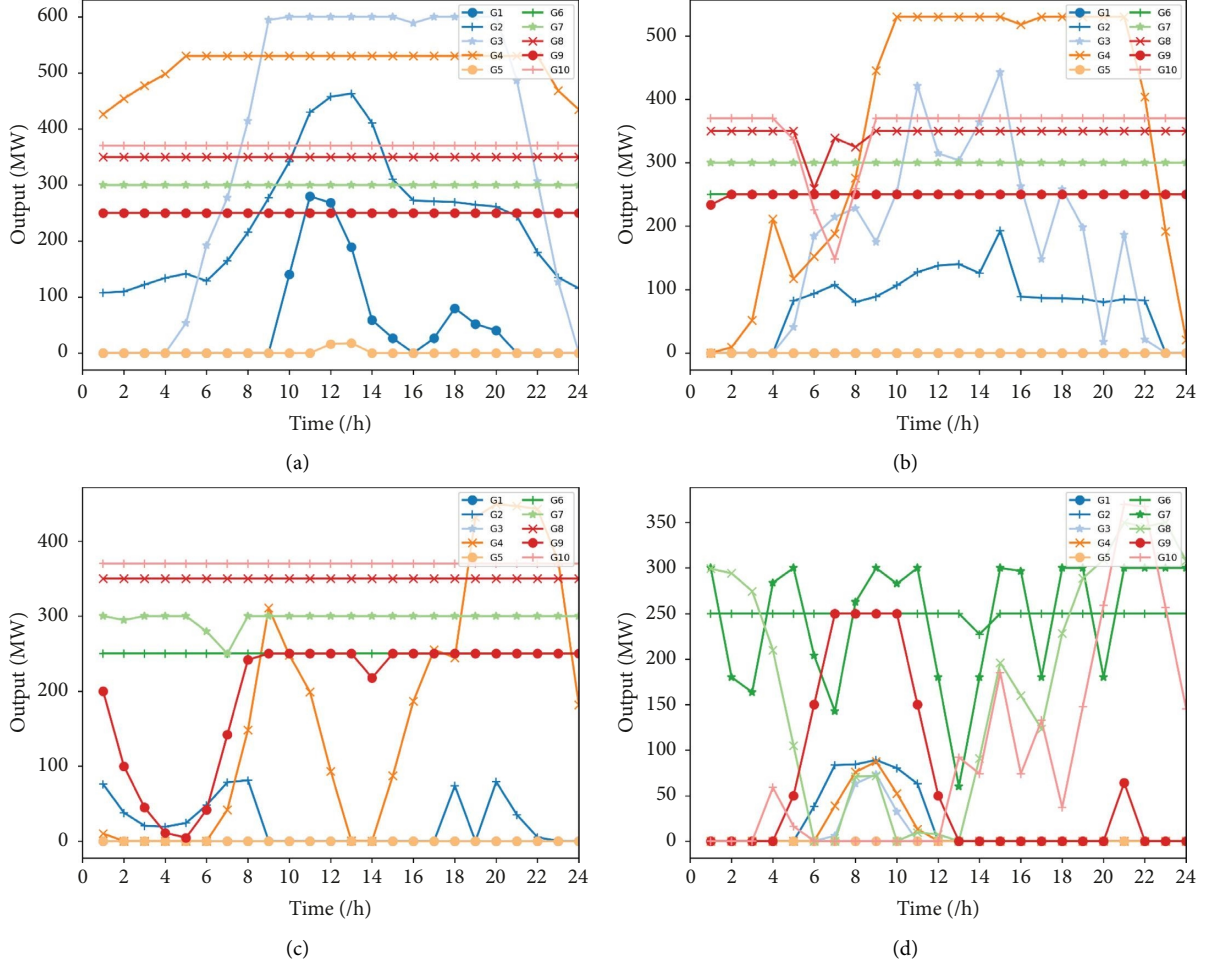| Type | Daily average (MW) | Standard deviation (MW) |
| --- | --- | --- |
| 1 | 517.60 | 97.57 |
| 2 | 1132.03 | 141.17 |
| 3 | 862.02 | 120.21 |
| 4 | 1195.51 | 65.11 |
| Average | 926.79 | 121.02 |



FIGURE 7: Thermal generator output. (a) Type 1. (b) Type 2. (c) Type 3. (d) Type 4.
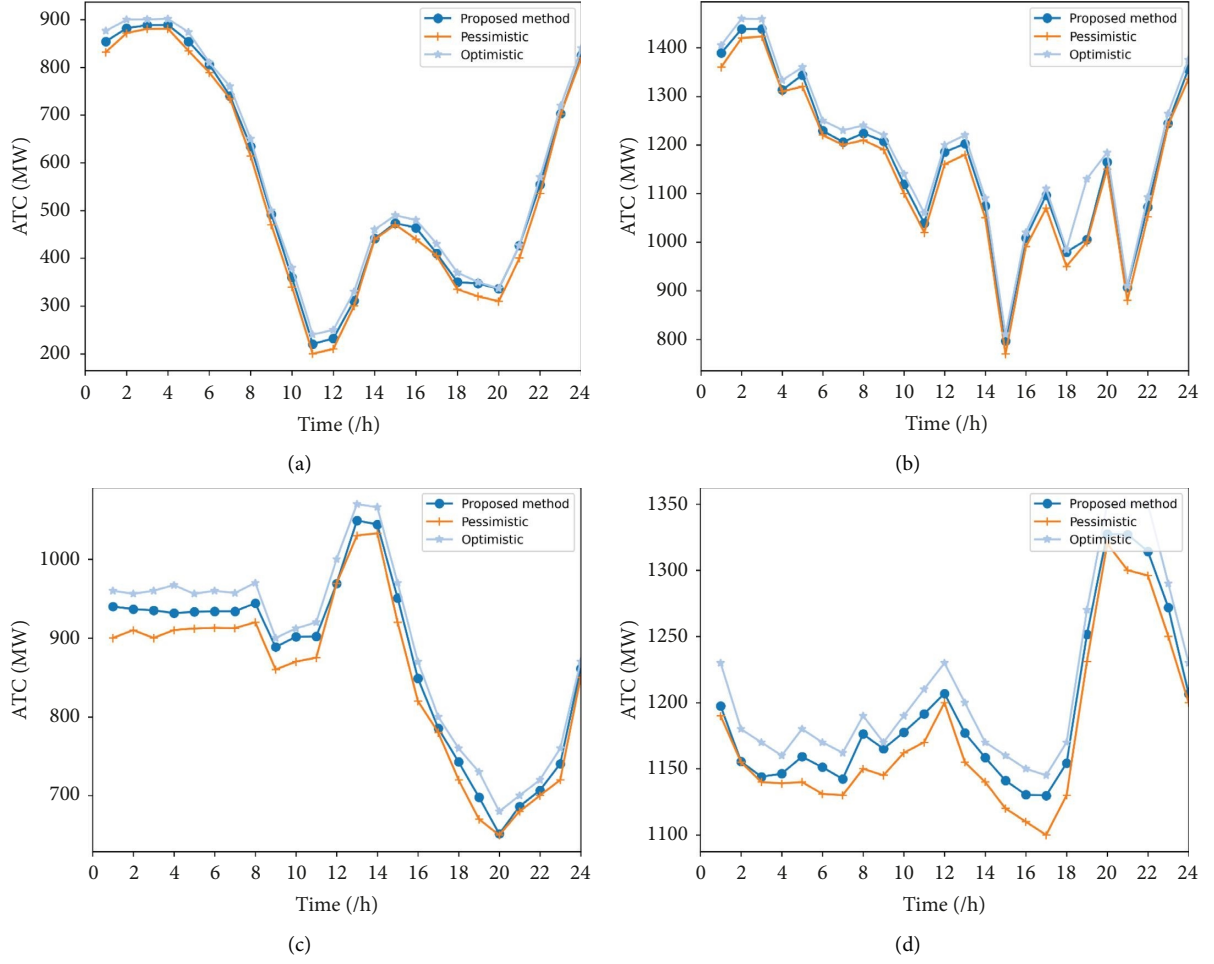
(a)

(b)

(c)

(d)

FIGURE 8: Comparison with the interval optimization method. (a) Type 1. (b) Type 2. (c) Type 3. (d) Type 4.
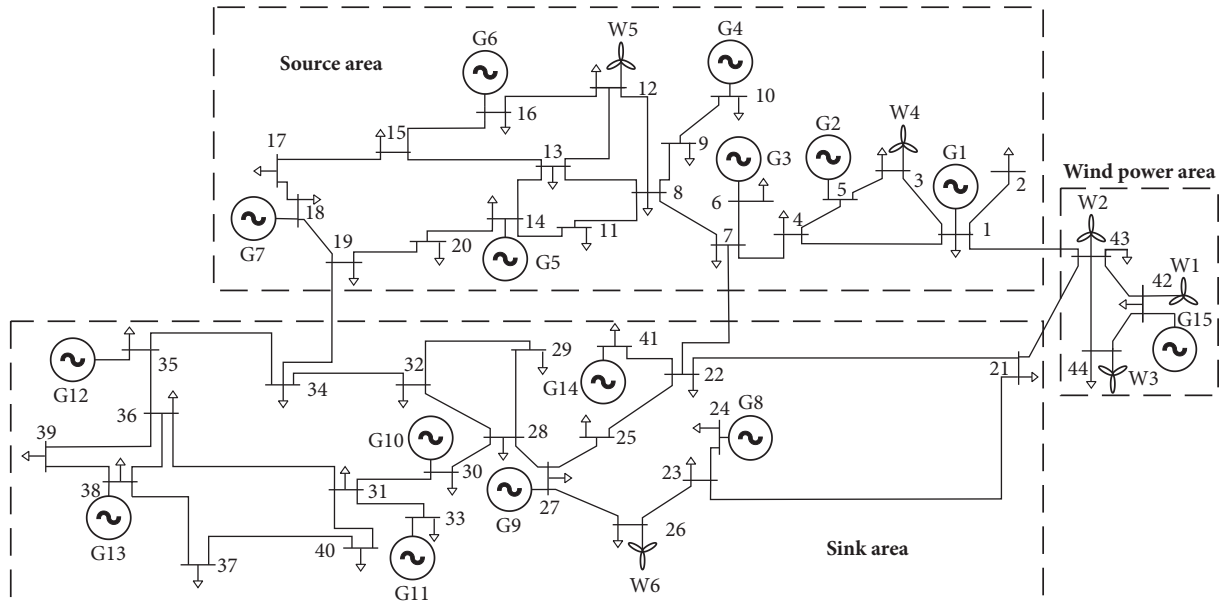


FIGURE 9: Real-world provincial power system diagram.

TABLE 4: Thermal power plant parameters for the 49-node system.

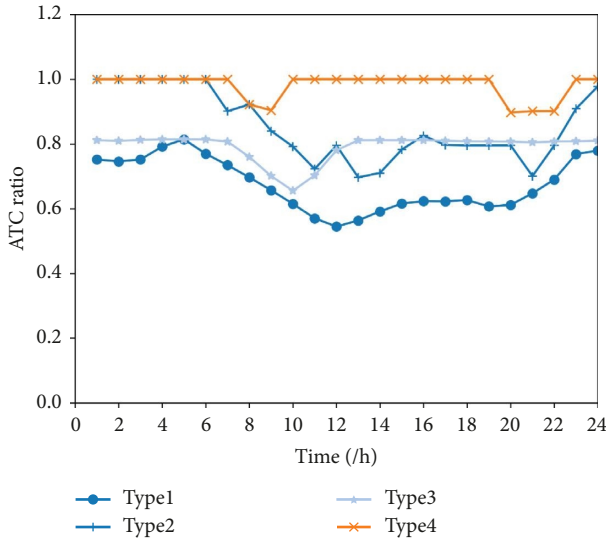| Bus no. | $c$ | $P_{\max}$ (MVA) | $P_{\min}$ (MVA) |
| --- | --- | --- | --- |
| $G_1$ | 1.2 | 2652 | 100 |
| $G_2$ | 1 | 2280 | 220 |
| $G_3$ | 2 | 1280 | 170 |
| $G_4$ | 1.5 | 1100 | 300 |
| $G_5$ | 1.5 | 1100 | 100 |
| $G_6$ | 2 | 1280 | 70 |
| $G_7$ | 1.5 | 1455 | 180 |
| $G_8$ | 1 | 360 | 50 |
| $G_9$ | 5 | 3252 | 300 |
| $G_{10}$ | 1 | 1280 | 70 |
| $G_{11}$ | 1.2 | 370 | 40 |
| $G_{12}$ | 1.5 | 1100 | 100 |
| $G_{13}$ | 2 | 430 | 40 |
| $G_{14}$ | 1.2 | 1570 | 200 |
| $G_{15}$ | 5 | 3252 | 300 |



FIGURE 10: Day-ahead ATC evaluation result.

## 5. Conclusion

Accurate and efficient online assessment of ATC of tie lines, especially renewable energy sending lines, is quite essential for the power market operation and renewable energy consumption. This paper proposes a probabilistic ATC assessment model considering the renewable energy and load uncertainty. With the multiobjective of thermal power plant cost and tie line ATC, the model is conducted with a set of stochastic renewable energy generation and load demand. Therefore, the transmission margin of tie lines is fully evaluated under the operation uncertainty. Furthermore, the scenario-based method overcomes the problem of conservative evaluation in the traditional method. The case studies of the IEEE standard system and real-world system suggest that a larger regional mismatch between the power output and the load demand leads to a lower ATC. In a power system with high renewable energy penetration, this mismatch is larger and the ATC tends to fluctuate more seriously.

Future works will also consider the frequency security constraint and N-1 contingency in ATC assessment, which can represent a more realistic operating condition of the power system [29].

## Nomenclature

| | |
| --- | --- |
| ATC: | Available transfer capability |
| $G$: | The set of nodes where the generators need to be adjusted |
| $P_{i,t}^m/Q_{i,t}^m$: | Active/reactive power output of the generator at node $i$ at time $t$ in the maximum transfer case |
| $c_i$: | The unit power generation cost of generator $i$ |
| $ATC_s$: | Daily available transfer capability of the system under typical daily scenario $s$ |
| $P_{i,t}^W$: | Active power output of the wind farm at node $i$ at time $t$ |
| $\lambda_i$: | The ratio of active nodal load and reactive nodal load |
| $S_{ij}^{\max}$: | The upper capability limit of line $(i, j)$ |
| $V^{\max}/V^{\min}$: | The upper limit/lower limit of the voltage of each PQ node |
| SR: | The set of nodes in the source area |
| $B_{ij}^1/B_{ij}^2$: | Equivalent admittance |
| $S^D$: | The set of load demand ratio |
| $\mathbb{P}_X$: | The true distribution of the observation |
| $\mathbb{P}_G$: | The distribution of random noise $z$ generator |
| $G(\cdot; \theta^{(G)})$: | The generator function, the symbol $\theta$, can be suppressed for convenience |
| $L_G/L_D$: | Loss function for the generator and discriminator |
| $W(A, B)$: | The Wasserstein distance between $A$ and $B$ |
| $W/D$: | The set of wind power integration node/load nodes |
| $P_{i,t}^G/Q_{i,t}^G$: | Active/reactive power output of the generator at node $i$ at time $t$ in the baseline case |
| $\alpha/\beta$: | The weight coefficients of the multiobjective optimization model |
| $P_{i,t}/Q_{i,t}$: | Active/reactive power injection at node $i$ at time $t$ |
| $P_{i,t}^D/Q_{i,t}^D$: | Active/reactive nodal load of node $i$ at time $t$ |
| $\delta_{i,t}/V_{i,t}$: | Phase/and amplitude of the voltage of node $i$ at time $t$ |
| $r_{ij}/x_{ij}$: | Resistance/reactance of line $(i, j)$ |
| $P_i^{Gmax}/P_i^{Gmin}$: | The upper limit/lower limit of power output for each generator |
| SK: | The set of nodes in the sink area |
| $S^W$: | The set of wind power plant output |
| $x_j^t$: | The vector of historical data indexed by time $t \in T$ |
| $\mathbb{P}_Z$: | The distribution of random noise $z$ |
| $\theta^{(G)}/\theta^{(D)}$: | The weights of the generator and discriminator network |
| $D(\cdot; \theta^{(D)})$: | The discriminator function, the symbol $\theta$, can be suppressed for convenience |
| $y$: | Condition label value. |

## Data Availability

The data that support the findings of this study are partially available in the main context of this article. The details of data availability are described as follows: the testing system diagram, generator cost coefficient, generator output limit, and load/wind power curve are presented in Section 4. The impedance data of the IEEE 9-bus system are open to the public, while the impedance data of real-world systems are not available due to the confidentiality provisions.

## Conflicts of Interest

The authors declare that there are no conflicts of interest.

## Authors' Contributions

Xiangfei Meng and Lina Zhang conceptualized the study, proposed the methodology, simulated the study, and wrote the manuscript. Xin Tian conceptualized the study and supervised the study. Hongqing Chu conceptualized the study and collected the field data. Yao Wang collected the field data. Qingxin Shi conceptualized the study.

## Acknowledgments

## References

[1] A. Kumar and S. Srivastava, "AC power transfer distribution factors for allocating power transactions in a deregulated market," *IEEE Power Engineering Review*, vol. 22, no. 7, pp. 42-43, 2002.

[2] H. Chen, X. He, T. Jiang, X. Fu, X. Li, and G. Li, "Available transfer capability calculation of power systems considering interruptible load," *Automation of Electric Power Systems*, vol. 41, no. 15, pp. 81–87+106, 2017.

[3] North American Electric Reliability Council, *Standard MOD-001-2—Modeling, Data, and Analysis—Available Transmission System Capacity*, North American Electric Reliability Council, Atlanta, GA, USA, 2014.

[4] A. M. Alshamrani, M. A. El-Meligy, M. A. F. Sharaf, W. A. Mohammed Saif, and E. M. Awwad, "Transmission expansion planning considering a high share of wind power to maximize available transfer capability," *IEEE Access*, vol. 11, pp. 23136–23145, 2023.

[5] Y. Ou and C. Singh, "Assessment of available transfer capability and margins," *IEEE Transactions on Power Systems*, vol. 17, no. 2, pp. 463–468, 2002.

[6] F. Wang and X. Bai, "OPF based transfer capability calculation," *Proceedings of the CSEE*, vol. 22, no. 11, pp. 16–41, 2002.

[7] B. Wang, X. Fang, X. Zhao, and H. Chen, "Bi-level optimization for available transfer capability evaluation in deregulated electricity market," *Energies*, vol. 8, no. 12, pp. 13344–13360, 2015.

[8] T. Jiang, X. Li, X. Kou, R. Zhang, G. Tian, and F. Li, "Available transfer capability evaluation in electricity-dominated integrated hybrid energy systems with uncertain wind power: an interval optimization solution," *Applied Energy*, vol. 314, Article ID 119001, 2022.

[9] Y. Huang, T. Ding, P. Wang et al., "Linearized AC power flow model based interval total transfer capability evaluation with uncertain renewable energy integration," *International Journal of Electrical Power and Energy Systems*, vol. 154, Article ID 109440, 2023.

[10] S. Madadi, B. Mohammadi-Ivatloo, and S. Tohidi, "Probabilistic available transfer capability evaluation considering dynamic line rating based on a sequential game-theoretic approach," *IEEE Systems Journal*, vol. 16, no. 1, pp. 891–901, 2022.

[11] X. Kou and F. Li, "Interval optimization for available transfer capability evaluation considering wind power uncertainty," *IEEE Transactions on Sustainable Energy*, vol. 11, no. 1, pp. 250–259, 2020.

[12] Y. Yang, F. Wen, L. Li, K. Wang, and X. Yang, "Coordinated model for available transfer capability decision-making employing multi objective chance constrained programming," *Automation of Electric Power Systems*, vol. 35, no. 13, pp. 37–43, 2011.

[13] H. Chen, X. Fang, R. Zhang, T. Jiang, G. Li, and F. Li, "Available transfer capability evaluation in a deregulated electricity market considering correlated wind power," *IET Generation, Transmission & Distribution*, vol. 12, no. 1, pp. 53–61, 2017.

[14] X. Li, J. Li, R. Zhang, X. Li, and M. Wang, "Probabilistic available transfer capability assessment in power system considering conditional value-at-risk and correlated wind power," *Transactions of China Electrotechnical Society*, vol. 38, no. 15, pp. 4162–4177, 2023.

[15] H. W. Reyad, M. Elfar, and E. E. El-Araby, "Probabilistic assessment of available transfer capability incorporating load and wind power uncertainties," *IEEE Access*, vol. 11, pp. 39048–39065, 2023.

[16] J. Liu and C. Chu, "Iterative distributed algorithms for real-time available transfer capability assessment of multiarea power systems," *IEEE Transactions on Smart Grid*, vol. 6, no. 5, pp. 2569–2578, 2015.

[17] P. Li, L. Zhu, X. Bai, and H. Wei, "Available transfer capability calculation constrained with small-signal stability based on adaptive gradient sampling," *Complexity*, vol. 2020, , Article ID 3912717, 10 pages, 2020.

[18] Y. Bao, J. Zhang, Y. Jiang, W. Xu, M. Bi, and J. Yang, "Online assessment method of available transfer capacity considering uncertainties of renewable energy output," *Electric Power Automation Equipment*, vol. 40, no. 4, pp. 71–76, 2020.

[19] A. M. Alshamrani, M. A. El-Meligy, M. A. F. Sharaf, W. A. Mohammed Saif, and E. M. Awwad, "Transmission expansion planning considering a high share of wind power to maximize available transfer capability," *IEEE Access*, vol. 11, pp. 23136–23145, 2023.

[20] J. Wei, G. Li, and M. Zhou, "Monte Carlo simulation and bootstrap method based assessment of available transfer capability in AC–DC hybrid systems," *International Journal of Electrical Power & Energy Systems*, vol. 53, pp. 231–236, 2013.

[21] Iso New England, "ISO new England calculation of TTC for external interfaces and ATC for PTF interfaces," 2009, http://www.oasis.oati.com/NU/NUdocs/iso_ne_ttc_atc_method.doc.

[22] H. Yuan, F. Li, Y. Wei, and J. Zhu, "Novel linearized power flow and linearized OPF models for active distribution networks with application in distribution LMP," *IEEE Transactions on Smart Grid*, vol. 9, no. 1, pp. 438–448, 2018.

[23] Q. Shi, F. Li, M. Olama et al., "Network reconfiguration and distributed energy resource scheduling for improved distribution system resilience," *International Journal of Electrical Power and Energy Systems*, vol. 124, pp. 1–10, 2021.

[24] S. Zhang, W. Liu, H. Wan et al., "Combing data-driven and model-driven methods for high proportion renewable energy distribution network reliability evaluation," *International Journal of Electrical Power and Energy Systems*, vol. 149, Article ID 108941, 2023.

[25] Y. Chen, Y. Wang, D. Kirschen, and B. Zhang, "Model-free renewable scenario generation using generative adversarial networks," *IEEE Transactions on Power Systems*, vol. 33, no. 3, pp. 3265–3275, 2018.

[26] T. Tieleman and G. Hinton, "Divide the gradient by a running average of its recent magnitude. COURSERA: neural networks for machine learning," *Technical report*, vol. 4, no. 2, pp. 26–31, 2012.

[27] M. Arjovsky, S. Chintala, and L. Bottou, "Wasserstein generative adversarial networks," *International conference on machine learning*, vol. 70, pp. 214–223, 2017.

[28] L. Zhao, X. Meng, L. Yang, and J. Wei, "Unified multi-objective optimization for regional power systems with unequal distribution of renewable energy generation and load," *Engineering Reports*, vol. 5, no. 10, 2023.

[29] M. Kenedy, R. Naresh, and R. Chauhan, "An efficient Repeated Power Flow approach to evaluate Available Transfer Capability considering power systems security," in *2023 Second International Conference on Electrical, Electronics, Information and Communication Technologies (ICEEICT)*, pp. 1–5, Trichirappalli, India, April 2023.